Heavy QCD axion in $b \to s$ transition: Enhanced limits and projections

Sabyasachi Chakraborty,[1,*] Manfred Kraus,[1,†] Vazha Loladze,[1,‡] Takemichi Okui,[1,2,§] and Kohsaku Tobioka[1,2,‖]

[1]*Department of Physics, Florida State University, Tallahassee, Florida 32306, USA*

[2]*Theory Center, High Energy Accelerator Research Organization (KEK), Tsukuba 305-0801, Japan*

(Received 9 March 2021; accepted 29 July 2021; published 24 September 2021)

We study a "heavy" QCD axion whose coupling to the standard model is dominated by $aG\tilde{G}$ but with $m_a \gg m_\pi f_\pi / f_a$. This is well motivated as it can solve the strong CP problem while evading the axion quality problem. It also poses interesting challenges for its experimental search due to its suppressed couplings to photons and leptons. Such axion with mass around a GeV is kinematically inaccessible or poorly constrained by most experimental probes except B-factories. We study $B \to Ka$ transitions as a powerful probe of the heavy QCD axion by performing necessary 2-loop calculations for the first time, together with some improvement on the existing analysis strategy. We find some of the existing limits are enhanced by at least an order of magnitude. We also demonstrate that the bounds are robust against unknown UV physics. For forthcoming data sets of the Belle II experiment, we provide a projection that f_a of a few TeV is within its future reach, which is relevant to the quality problem.

DOI: 10.1103/PhysRevD.104.055036

I. INTRODUCTION

Null signals of new physics at the TeV scale so far suggest us to adopt broader perspectives on the priorities of theoretical questions and future experimental programs. In particular, the possibility of new physics at scales much lighter than the TeV scale has been gaining growing attention. The axion offers a strong motivation for such light new physics, being a compelling solution [1,2] to the long-standing strong CP problem [3] by utilizing the Peccei-Quinn (PQ) symmetry [4,5], as well as being a candidate for cold dark matter [6–8].

The original axion model [1,2], in which QCD is the sole origin of the axion mass, predicts the relation $m_a f_a \simeq m_\pi f_\pi$ among the axion mass m_a, its decay constant f_a, and the analogous quantities for the pion. If we imagine that the PQ symmetry breaking scale, f_a, is related to the origin of the electroweak symmetry breaking, it would be natural to place f_a at the TeV scale, as proposed in the original axion models by Weinberg [1] and Wilczek [2], which then puts m_a at the keV scale by the relation above. This possibility, however, is excluded by astrophysical observations [9–12] and beam dump experiments [13–15]. Much higher f_a around $10^9 - 10^{13}$ GeV, and hence much lighter m_a, can be motivated by an axion as cold dark matter [16]. This part of the parameter space has also been searched with null results [17–19].

The relation, $m_a f_a \simeq m_\pi f_\pi$, can easily be violated, however, if there are additional contributions to the axion mass [20–37]. This permits us to reconsider the case where f_a is at or moderately above the TeV scale, but now with m_a much heavier than $\sim m_\pi f_\pi / f_a \sim$ keV. (It would be difficult, if not impossible, to imagine a scenario where m_a is *lighter* than $\sim m_\pi f_\pi / f_a$.) It is particularly important to explore the masses of 10 MeV $\lesssim m_a$ with TeV-scale f_a [38]. Such low values of f_a can also be motivated theoretically as a solution to the axion quality problem. If the violation of global symmetries by quantum gravity appears as unsuppressed $O(1)$ coefficients times powers of $f_a / M_{\rm Pl}$, the axion solution to the strong CP problem would be ruined [39–42] *unless* f_a is below $\sim$10 TeV [32].

In this work, therefore, we focus on what we call the *heavy QCD axion* scenario, where m_a is much heavier than $\sim m_\pi f_\pi / f_a$ and the axion couples to the SM dominantly via only the $aG_{\mu\nu}\tilde{G}^{\mu\nu}$ interaction, where a is the axion field and $G_{\mu\nu}$ the gluon field strength. Our effective Lagrangian thus has the form

$$\mathcal{L} = \mathcal{L}_{\rm SM} + \frac{\alpha_s}{8\pi}\frac{a}{f_a} G^a_{\mu\nu}\tilde{G}^{a\mu\nu} + \frac{1}{2}(\partial_\mu a)^2 - \frac{m_a^2}{2}a^2, \quad (1)$$

where $\tilde{G}^{a\mu\nu} \equiv \frac{1}{2}\epsilon^{\mu\nu\rho\sigma}G^a_{\rho\sigma}$. The additional terms required for renormalization that are phenomenologically relevant will

*schakraborty5@fsu.edu
†mkraus@hep.fsu.edu
‡vloladze@fsu.edu
§tokui@fsu.edu
‖ktobioka@fsu.edu

be discussed shortly. There are many models that UV-complete this EFT or could do so with minor modifications [30,32–34,36,37].

The status of experimental probes into the heavy QCD axion is the following. For $m_a \lesssim 400$ MeV, f_a at the TeV scale is excluded by the hadronic production and diphoton decay of the heavy axion, the proton beam dump experiment [15,43], the kaon experiments [44–52], the precision measurement of pion decay [53–55], the fixed target experiment [43,56,57], and the collider experiments [43,58,59]. For $m_a \gtrsim 400$ MeV, the search is difficult because the hadronic decay mode dominates, and it is overall poorly explored until m_a reaches 50 GeV where the CMS dijet search kicks in [38,60]. However, axion production from hadron decays such as $\phi \to \gamma a$ and $\eta' \to \pi\pi a$ constrain some parameter space [61] (see also Fig. 4). A part of the experimental loophole, $m_a \gtrsim 2$ GeV, can be explored at the LHC if the axion can decay into diphotons [62,63].

We thus see that the heavy QCD axion with m_a in the few GeV range and f_a at the TeV scale and above has not been explored. In this region, B physics should play a crucial role, having the right energy scale as well as great experimental precision. Moreover, the experimental reach of B physics will be improved further in upcoming years by LHCb ($300\ \text{fb}^{-1}$) and Belle II (5×10^{10} B-meson pairs). A promising channel is $B \to Ka$ with the axion subsequently decaying to hadrons, which is induced at 2-loop,[1] starting from the tree-level Lagrangian (1). The importance of this channel was pointed out in [43,66], but the required 2-loop calculation has not been performed to date. The previous work [43] relies on order of magnitude estimation for axion production.

Our goal, therefore, is to perform this calculation and obtain robust and competitive bounds for the heavy QCD axion. We will also provide a projection for the reach of Belle II.

II. CALCULATION OF $b \to sa$

Starting from the Lagrangian (1), the leading contribution to $b \to sa$ arises at 2-loop as shown in Fig. 1. Cancelling UV divergences in these diagrams requires the following additional interactions to be further included in the Lagrangian:

$$\mathcal{L} = \cdots + C_{qq} \sum_q \frac{\partial_\mu a}{f_a} \bar{q} \gamma^\mu \gamma_5 q + C_{bs} \frac{\partial_\mu a}{f_a} \bar{s}_L \gamma^\mu \gamma_5 b_L + \text{H.c.}, \tag{2}$$

where the ellipses denote the terms in Eq. (1) as well as those irrelevant for the $b \to sa$ phenomenology of our interest [see, e.g., [67,68] for those other operators generated at 1-loop from Eq. (1)]. The C_{qq} term is generated at 1-loop from the diagram shown in Fig. 2 and necessary to cancel 1-loop sub-divergences in Fig. 1. The C_{bs} term is required to remove remaining divergences at 2-loop. We have written the same coefficient C_{qq} for all quark flavors because we assume $m_t/\Lambda_{\text{UV}} \ll 1$ and ignore corrections of order $\sim m_t^2/\Lambda_{\text{UV}}^2$, where Λ_{UV} is the cutoff of our EFT.

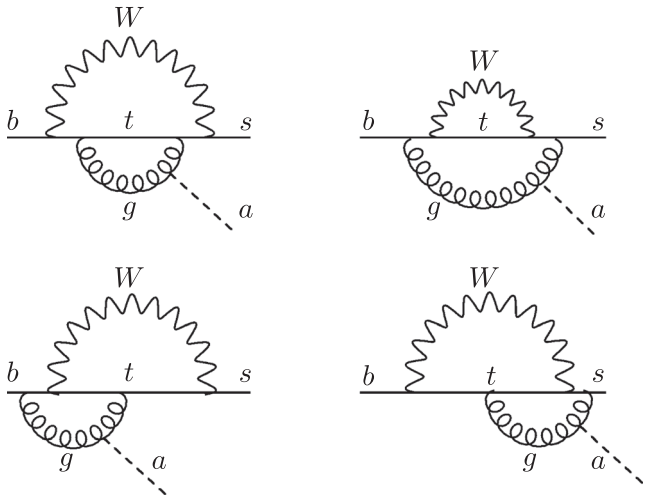

FIG. 1. Leading 1-particle-irreducible diagrams for $b \to sa$ from the Lagrangian (1).

It is not necessary at the 2-loop level to modify the coefficient of $aG\tilde{G}$ in Eq. (1) from $\alpha_s/8\pi f_a$, provided that the α_s here is treated as the running coupling $\alpha_s(\mu)$. While this claim is verified by an explicit calculation in the Appendix, it may be understood as follows. If we treat the axion as an external field, the coefficient of $(a/f_a)G\tilde{G}$ is completely fixed by matching the PQ-QCD-QCD anomaly. All corrections from turning a back on as a dynamical field involve the $aG\tilde{G}$ coupling itself at least twice and hence negligibly small.

Although C_{qq} and C_{bs} are free parameters in the EFT, their sizes must be consistent with the defining feature of our framework that the $aG\tilde{G}$ interaction is the dominant coupling of the axion to the SM. As we would set C_{qq} and

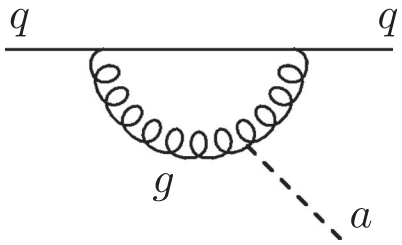

FIG. 2. The diagram that generates the C_{qq} term of Eq. (2).

[1]If there is an $aW\tilde{W}$ coupling, $b \to sa$ is induced at one-loop level [64] (see also [65]).

C_{bs} to zero for our scenario if there were no UV divergences requiring their presence as counter-terms, we regard them as having sizes roughly similar to the coefficients of the corresponding divergences (i.e., those of the $1/\epsilon$ poles in dimensional regularization). We thus take $C_{qq} \sim C_F(\alpha_s/4\pi)(g_s^2/16\pi^2) = C_F(\alpha_s/4\pi)^2$ (see Fig. 2) with $C_F = 4/3$. For C_{bs}, we further include two electroweak gauge couplings and GIM suppression (see Fig. 1), so $C_{bs} \sim C_F(\alpha_s/4\pi)^2(\alpha_w/4\pi)\sum_k V_{kb}V_{ks}^*\xi_k$, where V is the CKM matrix and $\xi_k \equiv m_k^2/M_W^2$ with $k = u, c, t$. Therefore, at the cutoff $\Lambda_{\rm UV}$ of our EFT, where it is matched on to the UV theory, we parametrize C_{qq} and C_{bs} as

$$C_{qq}(\Lambda_{\rm UV}) \equiv AC_F\left(\frac{\alpha_s}{4\pi}\right)^2,$$
$$C_{bs}(\Lambda_{\rm UV}) \equiv BC_F\left(\frac{\alpha_s}{4\pi}\right)^2\frac{\alpha_w}{4\pi}\sum_k V_{ik}V_{kj}^*\xi_k, \tag{3}$$

where A and B are $O(1)$ parameters that depends on the unknown UV completion of the Lagrangian in Eq. (1). All the SM parameters are evaluated at $\Lambda_{\rm UV}$. We will show, however, that our bounds on f_a are fairly insensitive to the exact values of A and B. Then, keeping in mind these rough sizes of C_{qq} and C_{bs}, we find the leading RG running of C_{qq} and C_{bs} (see Appendix for the details of the calculation):

$$\mu\frac{dC_{qq}}{d\mu} = -6C_F\left(\frac{\alpha_s}{4\pi}\right)^2, \tag{4}$$

$$\mu\frac{dC_{bs}}{d\mu} = \left(3C_F\left(\frac{\alpha_s}{4\pi}\right)^2 + C_{qq}\right)\frac{\alpha_w}{4\pi}\sum_k \xi_k V_{kb}V_{ks}^*. \tag{5}$$

After running down to $\mu \sim M_W$ using Eqs. (4), (5), we switch to another EFT in which the top quark and W boson are integrated out. In the limit of $m_{b,s}/M_W \to 0$, this new EFT contains only one operator relevant for the $b \to sa$ phenomenology:

$$\mathcal{L}_{bsa} = C_W\frac{\partial_\mu a}{f_a}\bar{s}_L\gamma^\mu\gamma_5 b_L + \text{H.c.}, \tag{6}$$

where C_W is determined by $C_{qq}(\mu_w)$ and $C_{bs}(\mu_w)$ with $\mu_w \sim M_W$ and the contributions from integrating out t and W. We find

$$C_W = C_{bs}(\mu_w) + \frac{\alpha_w}{4\pi}C_{qq}(\mu_w)g(\mu_w) + \frac{1}{2}\frac{\alpha_w}{4\pi}\left(\frac{\alpha_s}{4\pi}\right)^2 f(\mu_w), \tag{7}$$

where g and f are 1- and 2-loop matching functions given respectively in Eqs. (B7), (B6) in Appendix. In the limit of $m_{b,s}/M_W \to 0$, C_W does not run between M_W to m_b. This is because in this particular limit, there is no mixing between $aG\tilde{G}$ and flavor changing axial-vector coupling. In Fig. 3 we show the 1st, 2nd, and 3rd terms of the right-hand-side of Eq. (7) as well as the net C_W, all as a function of $\Lambda_{\rm UV}$, assuming the initial condition $A = B = 0$ in Eq. (3). We observe that C_{bs}, i.e., the $b-s-a$ operator dominates the overall C_W and interferes destructively with C_{gg}, i.e., $a-g-g$ operator. The dominance of C_{bs} can be explained by the operator mixing under the RGE evolution; C_{bs} acquires leading logarithmic contributions $\sim \ln(\Lambda_{\rm UV}^2/M_W^2)$ and $\sim \ln^2(\Lambda_{\rm UV}^2/M_W^2)$ due to the mixing with $a-g-g$ and $a-q-q$ operators. Since $\ln(\text{TeV}^2/M_W^2) \approx 5$ is a relatively large number, C_{bs} dictates over others.

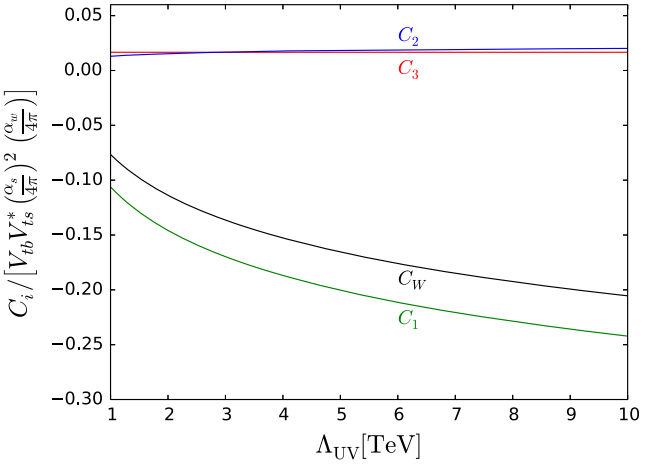

FIG. 3. C_1, C_2, and C_3 refers to the first, second, and third contribution in C_W respectively, for different UV scales [see Eq. (7)].

The final step is to evaluate the meson level decay $B \to aK^{(*)}$ [64,69]. We find

$$\Gamma_{B\to Ka} = |C_W|^2\frac{m_B^3}{64\pi f_a^2}\left(1-\frac{m_K^2}{m_B^2}\right)^2\lambda_{Ka}[f_0(m_a^2)]^2, \tag{8}$$

where λ_{Ka} is given by

$$\lambda_{Ka} = \left[\left(1-\frac{(m_K+m_a)^2}{m_B^2}\right)\left(1-\frac{(m_K-m_a)^2}{m_B^2}\right)\right]^{\frac{1}{2}}, \tag{9}$$

while $f_0(m_a^2)$ is the form factor obtained from the light-cone QCD sum rules [70,71]:

$$f_0(m_a^2) = \frac{0.330}{1-m_a^2/37.5\ \text{GeV}^2}. \tag{10}$$

It is important to note that these form factors derived from QCD sum rules have $O(10)\%$ uncertainties [70,71]. The approximate branching ratio is given by $\text{BR}(B^+ \to K^+a) \approx 1.1(7.6)\times 10^{-5}[f_a/100\ \text{GeV}]^2$ for $\Lambda_{\rm UV} = 1(10)$ TeV,

$A = B = 0$ and $m_a = 1$ GeV (the dependence of m_a is smaller than 10% in the parameter space we consider).

III. PHENOMENOLOGY

To derive constraints on the axion decay constant as a function of the mass we use different B decay measurements.

(i) We first derive the constraint on inclusive $b \to sa$ decay based on PDG data $\mathrm{BR}(B^+ \to \bar{c}X) = 97 \pm 4\%$ [72]. Thus, we require $\mathrm{BR}(b \to sa) < 1 - \mathrm{BR}(b \to c) \lesssim 11\%$. Note that this constraint does not contain any uncertainties coming from hadronization or calculation of axion decay. Therefore this is most robust bound derived in this paper. For inclusive branching fraction we use:

$$\mathrm{BR}(b \to sa) \simeq \frac{|C_W|^2}{\Gamma_B f_a^2} \frac{(m_B^2 - m_a^2)^2}{32\pi m_B}, \qquad (11)$$

where Γ_B is the width of B meson. The inclusive $b \to sa$ decay rules out the region marked by yellow in Fig. 4. In fact, this constraint is comparable and in some cases more robust than the bounds drawn for light meson phenomenology [43,47], e.g., $K_L \to \pi^0 a(\gamma\gamma)$, $\eta' \to \pi\pi a(3\pi)$, $\phi \to \gamma a(\pi\pi\gamma, \eta\pi\pi)$, and $\gamma p \to p a(\gamma\gamma)$, displayed in grey in Fig. 4.

(ii) Next we use exclusive final states $a \to 3\pi$, $\phi\phi$, $KK\pi$, and $\eta\pi\pi$ to perform axion search. We perform a peak search except in $a \to 3\pi$ final state. To calculate corresponding branching fractions for axion decay we use the data-driven approach given in Ref. [43] and use branching fractions given in Fig. 3 of their paper. The uncertainties in this approach for axion hadronic (partial) widths are not estimated in [43] so they are not included in the following bounds. However, these can be extracted by the same drive-driven method of Ref. [43].

(1) The constraints on the $a \to 3\pi$ channel, shown by the blue region in Fig. 4 is derived based on Belle analysis [73]. This analysis is applicable to $0.73\ \mathrm{GeV} \leq m_a \leq 0.83\ \mathrm{GeV}$. We require $\mathrm{BR}(B^0 \to K^0 a)\mathrm{BR}(a \to \pi^+\pi^-\pi^0) < 4.9 \times 10^{-6}$, which is from $\mathrm{BR}(B^0 \to K^0\omega) < 5.5 \times 10^{-6}$ [73] and $\mathrm{BR}(\omega \to \pi^+\pi^-\pi^0) = 89\%$.

(2) We use $B \to K\phi\phi$ data of *BABAR* [74] to derive a constraint on the $a \to \phi\phi$ channel, which is shown by the orange region in Fig. 4. We assume the axion to be at the center of each bin (see Fig. 5 of Ref. [74]) of width 125 MeV. Despite experimental smearing, the Gaussian event distribution coming from the axion decay is expected to be completely inside one of these bins. From the perspective of peak search, we also require the signal from the axion to be less than the central value of the measurement augmented with 2σ uncertainty.

(3) We analyze $B \to Ka(\to KK\pi)$ final state based on *BABAR* measurements [75]. The channel is studied at LHCb using 3 fb^{-1} data [76], but the sensitivity is currently weaker compared to *BABAR*. The bound is shown by the pink region in Fig. 4. To derive this

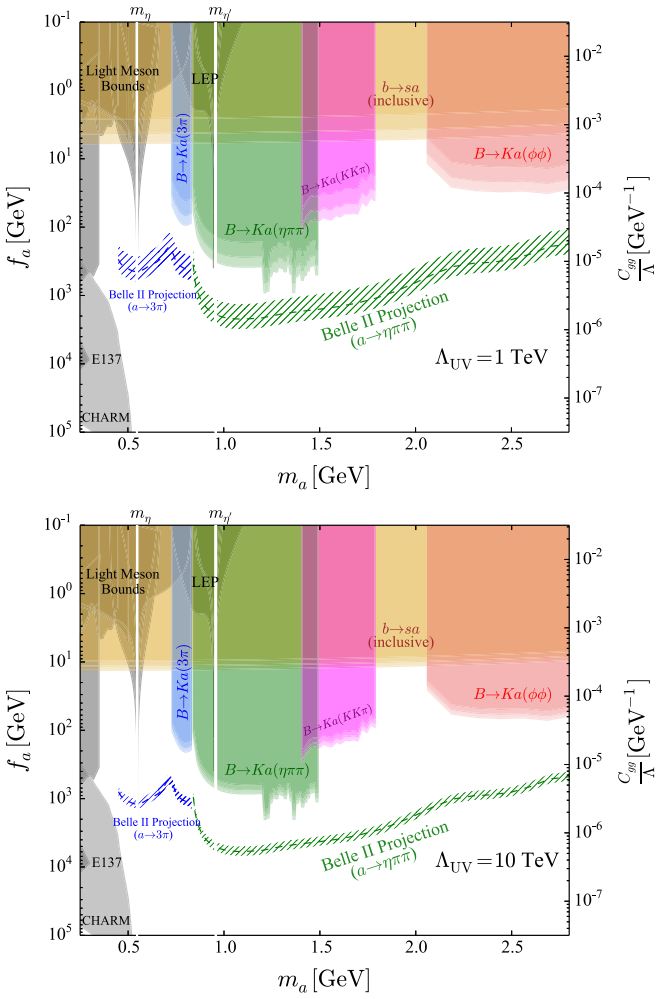

FIG. 4. We portray the constraints from different B-decay measurements in the $m_a - f_a$ plane. Three curves are drawn for each constraint corresponding to different initial conditions [see Eq. (3)], i.e., the strongest $(A = +3, B = -3)$, weakest $(A = -3, B = +3)$, and central constraints $(A = B = 0)$. We choose the UV scale $\Lambda_{\rm UV}$ to be 1 and 10 TeV for the top and the bottom plot, respectively. See main texts about systematic uncertainties from the form factor of Eq. (10) and the data-driven calculation of the axion branching fractions. The grey shaded regions comprise bounds from [13,15,43,47,52,57–59]. For $B \to Ka$, we use [72] for inclusive analysis and [73–75] for exclusive channels $a \to 3\pi, \eta\pi\pi, KK\pi, \phi\phi$. For the projection at Belle II (dashed lines), 5×10^{10} $\bar{B}B$ pair is assumed, and the band shows the dependence on the different initial conditions. The right vertical axis is labeled using the notation of Ref. [43] for comparison.

bound, we follow a similar strategy mentioned previously with one difference. The bin size for $KK\pi$ experimental data is only 22.5 MeV (see Fig. 1(e) of Ref. [75]). Hence, instead of assuming the axion mass to be at the center of each bin, we assume it to be at the boundary of adjacent bins. We then require the number of events from the decay of the axion to be less than the sum of central values of those two bins plus 2σ uncertainty, after subtracting nonresonant background from the measurement. The merging of two bins correct for any spilling over effect due to experimental smearing. Further, experimental efficiency is calculated based on binned data and final measurement of the branching fraction given on Fig. 1 (e) and Table I of [75] respectively. Finally, the data analysis performed on $KK\pi$ measurement contains mass cut: one of the $K\pi$ pair invariant mass is required to be $0.85\ \text{GeV} \lesssim m_{K\pi} \lesssim 0.95\ \text{GeV}$. To apply this cut on axion decay calculations we use $a \to KK\pi$ matrix element given in Eq. (S59-S61) of [43]. However, the result strongly depends on the experimental input parameters that have large uncertainties. Because of these uncertainties, bounds from this channel have order one error close to the end of the mass spectrum $m_a \sim 1.8$ GeV.

(4) For $a \to \eta\pi\pi$ [75] in the $1.2\ \text{GeV} < m_a < 1.5\ \text{GeV}$ window, we do everything similarly to $KK\pi$ except the mass cut. For $m_a < 1.2$ GeV one can notice that the number of measured events are less than for $m_a > 1.2$ GeV. Therefore, we take the weakest constraint from $m_a > 1.2$ GeV region and extend this branching ratio bound for low axion mass $m_a < 1.2$ GeV. As depicted by the green shaded region in Fig. 4, this channel provides the strongest constraint on the parameter space.

(i) Finally we derive Belle II projection for $a \to \eta\pi\pi$ and $a \to 3\pi$ search, shown as the green and blue dashed curves in Fig. 4.

(1) To estimate $a \to \eta\pi\pi$ projection we first extrapolate *BABAR*'s continuous QCD background given on FIG.1 (f) of [75]. Next, we scale it with luminosity, assuming 5×10^{10} $\bar{B}B$ pair at Belle II. Eventually, based on our result we calculate standard deviation and require that signal from the axion to be less than 2 times this standard deviation. We estimate the experimental resolution of the axion mass as $\delta m_a \sim \delta m_{\eta\pi\pi} m_a / m_{\eta'}$ where $\delta m_{\eta\pi\pi} \sim 13.4$ MeV is the experimental resolution of the η' mass fitted from the Fig. 1(f) of [75].

(2) To derive $a \to 3\pi$ projection we do everything similarly to $a \to \eta\pi\pi$ except we use Fig. 2(d) of [73], which shows background in $0.73\ \text{GeV} < m_a < 0.83\ \text{GeV}$ range. We assume background for $m_a < 0.73$ GeV to be same as at $m_a = 0.73$ GeV. Also, we use fixed $\delta m_a \approx 40$ MeV experimental resolution of the axion mass, that is estimated using the signal shape of ω shown on the same figure.

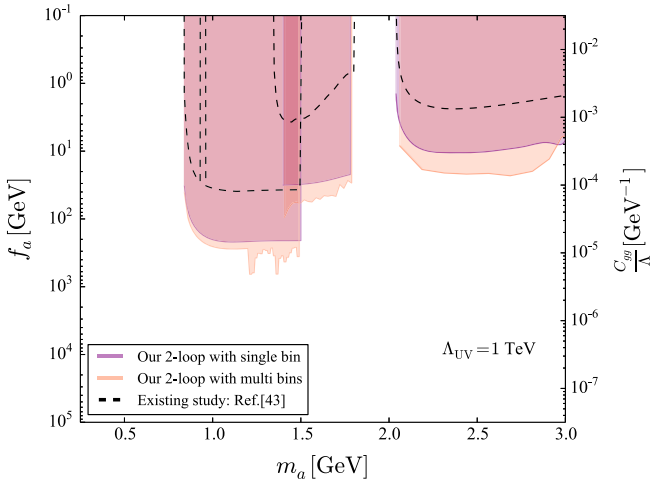

FIG. 5. In this figure, the dark red colored regions are obtained with our two loop amplitude. This shows a factor of 5 or 6 enhancement from the axion production rate compared to the previous estimation obtained in [43] (shown by the dashed lines). Both of these results use single bin analysis as mentioned in the text. Additional enhancement of factor 2, shown by the light red region, comes from our multiple bin analysis.

Finally, it is a nontrivial result of our study that the bounds on f_a are not very sensitive to the exact values of A and B, mainly because the double logarithmic enhancement we calculated in this paper dominate. This means that the bounds and projections obtained in our paper are independent of the exact nature of unknown UV physics. Moreover, since the uncertainties in the form factors (10) are $O(10)\%$, so our calculation also shows that the detail of UV physics is relatively a minor effect, particularly for large UV scales.

IV. CONCLUSION

In this paper, we performed the first 2-loop calculation for the axion production from $B \to Ka$ process starting from the minimal interaction of the QCD axion, $aG\tilde{G}$ (Eq. (1). Assuming the UV scale to be at 1 TeV, the constraints on the $m_a - f_a$ parameter space (see Fig. 4) turns out to be $\sim$10 times stronger than the previous estimate [43]. Increasing the UV scale only increases this difference. The reason for this enhancement is two fold. First, in [43] the amplitude was a rough estimate up to $O(1)$ factors in the coefficients and without the complete logarithmic enhancement. In contrast, our work, for the first time, provides the complete leading 2-loop amplitude with RG improvement for the axion-induced FCNC processes, which exhibits an enhancement by a factor of about 5 or 6 in the axion production rate. Secondly, we perform a detailed bin by bin analysis instead of assuming an overall

branching fraction. This makes our bound even more robust by roughly a factor of two at least and sometimes more as shown in Fig. 5. Combining these two effects, our bounds are enhanced by at least an order of magnitude with respect to the previous rough estimates in Ref. [43]. Therefore, the bounds on the decay constant is order of 100 GeV using Belle and *BABAR* measurements for $\Lambda_{\rm UV} = 1$ TeV. For the future, although there are many intensive studies for the heavy QCD axion based on the (near) future data at kaon factories [47], GlueX [57], LHC with track-trigger [35,77], DUNE near detector [78], or beam-dump type facilities (summarized in Fig. 41 of [79]), the $B \to Ka$ process is particularly important for GeV mass range of the axion. This is because the GeV axion is not produced at light meson precision experiments and also because the lifetime is shorter due to the hadronic decay channeling the beam-dump experiments less effective. Belle II will be able to cover the unique parameter space using $B \to Ka(\to \eta\pi\pi, 3\pi)$ as shown in Fig. 4, and we expect the other channels and future data of LHCb will further improve the sensitivities. Also, $B \to Ka(\to \gamma\gamma)$ will be another attractive channel particularly for $m_a < 3m_\pi \simeq 450$ MeV, which is not yet studied in B-factories.

ACKNOWLEDGMENTS

We thank Mike Williams and Yotam Soreq for correspondence regarding Ref. [43]. We also thank Lina Alasfar, Fernando Febres Cordero, Andrei Gritsan, TaeHyun Jung, and Abner Soffer for discussions. This work is supported by by the U.S. Department of Energy Grant No. DE-SC0010102.

APPENDIX A: RENORMALIZATION SCHEME

We start from the EFT Lagrangian:

$$\mathcal{L} = \mathcal{L}_{\rm SM} + \mathcal{L}_a + \sum_i C_i \mathcal{O}_i + \ldots, \tag{A1}$$

where $\mathcal{L}_a$ denotes the axion kinetic and potential terms and the ellipses represent effective operators irrelevant for the $b \to sa$ phenomenology of our interest, while $i \in \{gg, qq, bs\}$ and

$$\begin{aligned}
\mathcal{O}_{gg} &= \frac{1}{8\pi}\frac{a}{f_a} G^a_{\mu\nu}\tilde{G}^{a\mu\nu}, \\
\mathcal{O}_{qq} &= \sum_q \frac{\partial_\mu a}{f_a}\bar{q}\gamma^\mu\gamma_5 q, \\
\mathcal{O}_{bs} &= \frac{\partial_\mu a}{f_a}\bar{s}_L\gamma^\mu\gamma_5 b_L + \text{H.c.}.
\end{aligned} \tag{A2}$$

However, we will soon be redefining $\mathcal{O}_{qq}$ and $\mathcal{O}_{bs}$ below in order to take into account the subtleties of dealing with γ_5 in dimensional regularization (DR).

To simplify our calculations, we will neglect terms of order $m^2_{b,s,a}/M^2_W$ or higher. This in particular means that we evaluate the diagrams in Fig. 1 at vanishing external momenta. The Feynman gauge has been used throughout our calculations and thus the inclusion of an unphysical Nambu-Goldstone mode accompanying every W boson is implied in the following discussions. We have implemented tensor reduction in FORM [80] and used KIRA [81] to obtain integration-by-parts relations.

We will regulate UV divergences using DR, while we cut off IR divergences explicitly by introducing fictitious quark masses. Note that all diagrams in Fig. 1 as well as all coefficients in Eq. (7) are $O(\alpha_s^2\alpha_w)$. At this order, the dependence on the fictitious masses actually cancels out as the IR theory (6) has no IR divergences even in the $m_{b,s} \to 0$ limit at the same order. We have checked this cancellation explicitly as a validation of our calculations.

The absence of anomalous chiral fermion loops in the diagrams of Fig. 1 allows us to adopt the following simple prescription for γ_5 and $\epsilon^{\mu\nu\rho\sigma}$. We first redefine $\mathcal{O}_{qq}$ and $\mathcal{O}_{bs}$ as

$$\begin{aligned}
\mathcal{O}_{qq} &= \frac{\rm i}{6}\frac{\partial_\mu a}{f_a}\epsilon^{\mu\nu\rho\sigma}\sum_q \bar{q}\,\gamma_\nu\gamma_\rho\gamma_\sigma q, \\
\mathcal{O}_{bs} &= \frac{\rm i}{6}\frac{\partial_\mu a}{f_a}\epsilon^{\mu\nu\rho\sigma}\bar{s}_L\gamma_\nu\gamma_\rho\gamma_\sigma b_L + \text{H.c.},
\end{aligned} \tag{A3}$$

which is equivalent to their original forms in $d = 4$ but we use these new forms in $d = 4 - 2\epsilon$ because what we directly obtain from diagrams in Fig. 1 is actually the product of three γ matrices multiplied by the ϵ tensor from the $a - g - g$ vertex. Therefore, all we need is the total antisymmetric property of the ϵ tensor, which we assume as part of the definition of our scheme, and the property $\{\gamma_5, \gamma^\mu\} = 0$, which is valid as we have no anomalous chiral fermion loops. We do not use any explicit form of the ϵ tensor nor any relation between γ_5 and the ϵ tensor, until only after all divergences are cancelled and we are back to $d = 4$.

We employ the $\overline{MS}$ scheme (with one exception mentioned below) and redefine the Wilson coefficients as

$$C_i \to \sum_j (e^{\gamma_E}\mu^2/4\pi)^{\epsilon/2} C_j \gamma_{ji}, \qquad \mathcal{O}_i \to \sum_j \mathcal{Z}_{ij}\mathcal{O}_j, \tag{A4}$$

where $\mathcal{Z}$ consists of the field-strength renormalizations of the SM fields inside $\mathcal{O}_i$. For our 2-loop computation depicted in Fig. 1, it only has three nontrivial components:

$$\mathcal{Z} = \begin{pmatrix} Z_G & 0 & 0 \\ 0 & Z_q & Z_{bs} \\ 0 & 0 & 1 \end{pmatrix}, \tag{A5}$$

where Z_G and Z_q are respectively the gluon and quark field-strength renormalizations due to 1-loop QCD corrections,

while Z_{bs} the renormalization of the $b-s$ kinetic mixing induced by a W loop. We use $\overline{MS}$ to determine Z_G and Z_q, while we fix Z_{bs} by requiring that the net $b-s$ kinetic mixing should vanish at 1-loop at vanishing quark momentum.

All of these are determined completely by the SM and we find

$$\begin{aligned} Z_G &= 1+\frac{\alpha_s}{4\pi}\left(\frac{5}{3}N_c-\frac{2}{3}N_f\right)\frac{1}{\epsilon}, \\ Z_q &= 1-\frac{\alpha_s}{4\pi}\frac{C_F}{\epsilon}, \\ Z_{bs} &= -\frac{\alpha_w}{4\pi}\sum_k \frac{\xi_k V_{kb}V_{ks}^*}{4}\left[\frac{1}{\epsilon}-\ln\frac{M_W^2}{\mu^2}+\frac{3(\xi_k+1)}{2(\xi_k-1)}\right. \\ &\quad \left.-\frac{\xi_k(2+\xi_k)}{(\xi_k-1)^2}\ln\xi_k\right], \end{aligned} \tag{A6}$$

where $N_c=3$ and $N_f=6$.

APPENDIX B: ANOMALOUS DIMENSIONS AND RENORMALIZATION GROUP EVOLUTIONS

To obtain the anomalous dimensions matrix γ in Eq. (A4), we calculate 1- and 2-loop diagrams contributing to the $a-g-g$, $a-q-q$ and $a-b-s$ vertex corrections in $\overline{MS}$. We find

$$\gamma = \begin{pmatrix} 1-\frac{\alpha_s}{4\pi}\frac{\beta_0}{\epsilon} & -\frac{\alpha_s}{16\pi^2}\frac{3C_F}{\epsilon} & \frac{\alpha_s}{16\pi^2}\frac{\alpha_w}{4\pi}\frac{3C_F S}{4}\left(\frac{1}{\epsilon}-\frac{1}{\epsilon^2}\right) \\ 0 & 1 & \frac{\alpha_w}{4\pi}\frac{S}{2\epsilon} \\ 0 & 0 & 1 \end{pmatrix}, \tag{B1}$$

where $\beta_0 = 11N_c/3-2N_f/3$ and $S=\sum_k \xi_k V_{kb}V_{ks}^*$. The RGEs can then be found by demanding $\mu \mathrm{d}(\mu^\epsilon C_i \gamma_{ij})/\mathrm{d}\mu = 0$, i.e.,

$$\mu\frac{\mathrm{d}C_i}{\mathrm{d}\mu} = -\epsilon C_i - \sum_{j,k} C_j \mu \frac{\mathrm{d}\gamma_{jk}}{\mathrm{d}\mu}(\gamma^{-1})_{ki}. \tag{B2}$$

In the limit $\epsilon \to 0$, we get

$$\begin{aligned} \mu\frac{\mathrm{d}C_{gg}}{\mathrm{d}\mu} &= -\beta_0\frac{\alpha_s}{2\pi}C_{gg}, \\ \mu\frac{\mathrm{d}C_{qq}}{\mathrm{d}\mu} &= -6C_F\frac{\alpha_s}{4\pi}\frac{C_{gg}}{4\pi}, \\ \mu\frac{\mathrm{d}C_{bs}}{\mathrm{d}\mu} &= \left(3\frac{\alpha_s}{4\pi}\frac{C_{gg}}{4\pi}C_F + C_{qq}\right)\frac{\alpha_w}{4\pi}\sum_k \xi_k V_{kb}V_{ks}^*. \end{aligned} \tag{B3}$$

Here, to see the size of each contribution, recall that roughly $C_{gg}\sim\alpha_s$ and $C_{qq}\sim(\alpha_s/4\pi)^2$. We further simply the RGE for C_{bs} by neglecting the u and c quark masses. This then allows us to combine α_w and ξ_t as $\alpha_w\xi_t = y_t^2/2\pi$. Therefore, we also incorporate the SM running of the top-quark Yukawa coupling:

$$\mu\frac{\mathrm{d}y_t}{\mathrm{d}\mu} \simeq \frac{y_t}{16\pi^2}\left(\frac{9}{2}y_t^2-8g_3^2\right). \tag{B4}$$

We also take into account the running of V_{ts}. The leading contribution reads [82]

$$\mu\frac{\mathrm{d}V_{ts}}{\mathrm{d}\mu} \simeq \frac{3}{32\pi^2}y_t^2 V_{ts}. \tag{B5}$$

Let us first verify our claim in the main text that the running of C_{gg} is completely accounted for by the SM running of α_s. This can be trivially seen by solving Eq. (B3) with the initial condition $C_{gg}(\Lambda_{\mathrm{UV}})=\alpha_s(\Lambda_{\mathrm{UV}})$, which leads to $C_{gg}(\mu)=\alpha_s(\mu)$. Then, setting $C_{gg}(\mu)=\alpha_s(\mu)$ in the RGEs for C_{qq} and C_{bs} above, we obtain the results in Eq. (3).

After we run from Λ_{UV} down to $\mu\sim M_W$, we integrate out the W and t and match onto the EFT described by the operator (6) with the coefficient (7), where we find

$$\begin{aligned} f(\mu) = \frac{3}{2}C_F\sum_k V_{kb}V_{ks}^*\left[-\frac{3\xi_k}{2}\ln^2\frac{M_W^2}{\mu^2}+\left\{\frac{\xi_k(3\xi_k-2)(3\xi_k+4)}{2(\xi_k-1)^2}-\frac{(\xi_k-2)(3\xi_k+1)}{\xi_k-1}\ln(\xi_k-1)\right\}\ln\xi_k\right. \\ +\frac{3\xi_k^3-14\xi_k^2-8\xi_k+4}{2(\xi_k-1)^2}\ln^2\xi_k+\left\{\frac{9\xi_k(\xi_k+1)}{2(\xi_k-1)}-\frac{\xi_k(3\xi_k^2-2\xi_k+8)}{(\xi_k-1)^2}\ln\xi_k\right\}\ln\frac{M_W^2}{\mu^2} \\ +\frac{\pi^2(4+11\xi_k-7\xi_k^2)+3\xi_k(13\xi_k-3)}{12(\xi_k-1)}+\frac{(\xi_k-2)(3\xi_k+1)}{\xi_k-1}\mathrm{Li}_2\left(\frac{1}{\xi_k}\right) \\ \left.-\frac{(\xi_k+2)(\xi_k^2+2\xi_k-1)}{(\xi_k-1)^2}\mathrm{Li}_2\left(\frac{\xi_k-1}{\xi_k}\right)\right]. \end{aligned} \tag{B6}$$

$$g(\mu) = \frac{1}{4}\sum_k V_{kb}V_{ks}^*\xi_k\left[\frac{\xi_k+5}{\xi_k-1}+\frac{2(\xi_k^2-2\xi_k+4)}{(\xi_k-1)^2}\times\ln\xi_k+2\ln\frac{M_W^2}{\mu^2}\right]. \quad \text{(B7)}$$

We verified that the difference between Eq. (B7) and the 1-loop matching function found in Eq. (71) of Ref. [66] is due to different scheme choices of handling γ_5 and the Levi-Cevita tensor.

APPENDIX C: INPUT PARAMETERS

In Table I we list the input parameters used in our analysis.

TABLE I. Input parameters.

Parameters	Values
G_F [61]	1.166×10^{-5} GeV^{-2}
$\alpha_s(M_Z)$ [61]	0.1181 ± 0.002
V_{tb} [61]	0.9991
V_{ts} [61]	0.0413
M_W [61]	80.379 GeV
M_Z [61]	91.187 GeV
$\overline{m_t}(m_t)$ [83]	163.6 GeV
$\overline{m_b}(m_b)$ [61]	4.18 GeV
$\overline{m_s}(m_s)$ [61]	92.9 MeV
m_B [61]	5.279 GeV
$m_K^{\pm}$ [61]	493.6 MeV
m_K^0 [61]	497.6 MeV

[1] S. Weinberg, A new light boson?, Phys. Rev. Lett. **40**, 223 (1978).
[2] F. Wilczek, Problem of Strong P and T Invariance in the Presence of Instantons, Phys. Rev. Lett. **40**, 279 (1978).
[3] G. 't Hooft, Symmetry Breaking Through Bell-Jackiw Anomalies, Phys. Rev. Lett. **37**, 8 (1976).
[4] R. Peccei and H. R. Quinn, *CP* Conservation in the Presence of Instantons, Phys. Rev. Lett. **38**, 1440 (1977).
[5] R. Peccei and H. R. Quinn, Constraints imposed by *CP* conservation in the presence of instantons, Phys. Rev. D **16**, 1791 (1977).
[6] J. Preskill, M. B. Wise, and F. Wilczek, Cosmology of the invisible axion, Phys. Lett. **120B**, 127 (1983).
[7] M. Dine and W. Fischler, The Not So Harmless Axion, Phys. Lett. **120B**, 137 (1983).
[8] L. F. Abbott and P. Sikivie, A cosmological bound on the invisible axion, Phys. Lett. **120B**, 133 (1983).
[9] V. Anastassopoulos *et al.* (CAST Collaboration), New CAST limit on the axion-photon interaction, Nat. Phys. **13**, 584 (2017).
[10] G. G. Raffelt, Astrophysical axion bounds, Lect. Notes Phys. **741**, 51 (2008).
[11] G. G. Raffelt, *Stars as laboratories for fundamental physics: The astrophysics of neutrinos, axions, and other weakly interacting particles* (University of Chicago Press, 1996).
[12] A. Friedland, M. Giannotti, and M. Wise, Constraining the Axion-Photon Coupling with Massive Stars, Phys. Rev. Lett. **110**, 061101 (2013).
[13] J. Bjorken, S. Ecklund, W. Nelson, A. Abashian, C. Church, B. Lu, L. Mo, T. Nunamaker, and P. Rassmann, Search for neutral metastable penetrating particles produced in the SLAC beam dump, Phys. Rev. D **38**, 3375 (1988).
[14] J. Blumlein *et al.*, Limits on neutral light scalar and pseudoscalar particles in a proton beam dump experiment, Z. Phys. C **51**, 341 (1991).
[15] F. Bergsma *et al.* (CHARM Collaboration), Search for axion like particle production in $\{400-$ GeV$\}$ proton—copper interactions, Phys. Lett. **157B**, 458 (1985).
[16] J. E. Kim and G. Carosi, Axions and the strong *CP* problem, Rev. Mod. Phys. **82**, 557 (2010); Erratum, Rev. Mod. Phys. **91**, 049902 (2019).
[17] E. Arik *et al.* (CAST Collaboration), Probing eV-scale axions with CAST, J. Cosmol. Astropart. Phys. 02 (2009) 008.
[18] S. J. Asztalos *et al.* (ADMX Collaboration), Design and performance of the ADMX SQUID-based microwave receiver, Nucl. Instrum. Methods Phys. Res., Sect. A **656**, 39 (2011).
[19] S. Aune *et al.* (CAST Collaboration), CAST Search for sub-eV Mass Solar Axions with 3He Buffer Gas, Phys. Rev. Lett. **107**, 261302 (2011).
[20] S. Dimopoulos, A solution of the strong {CP} problem in models with scalars, Phys. Lett. B **84**, 435 (1979).
[21] B. Holdom and M. E. Peskin, Raising the axion mass, Nucl. Phys. **B208**, 397 (1982).
[22] M. Dine and N. Seiberg, String theory and the strong {CP} problem, Nucl. Phys. **B273**, 109 (1986).
[23] J. M. Flynn and L. Randall, A computation of the small instanton contribution to the axion potential, Nucl. Phys. **B293**, 731 (1987).
[24] K. Choi, C. W. Kim, and W. K. Sze, Mass Renormalization by Instantons and the Strong {CP} Problem, Phys. Rev. Lett. **61**, 794 (1988).
[25] V. A. Rubakov, Grand unification and heavy axion, JETP Lett. **65**, 621 (1997).
[26] K. Choi and H. D. Kim, Small instanton contribution to the axion potential in supersymmetric models, Phys. Rev. D **59**, 072001 (1999).
[27] Z. Berezhiani, L. Gianfagna, and M. Giannotti, Strong *CP* problem and mirror world: The Weinberg-Wilczek axion revisited, Phys. Lett. B **500**, 286 (2001).
[28] K.-w. Choi, A QCD Axion from Higher Dimensional Gauge Field, Phys. Rev. Lett. **92**, 101602 (2004).
[29] A. Hook, Anomalous Solutions to the Strong *CP* Problem, Phys. Rev. Lett. **114**, 141801 (2015).
[30] H. Fukuda, K. Harigaya, M. Ibe, and T. T. Yanagida, Model of visible QCD axion, Phys. Rev. D **92**, 015021 (2015).

[31] S. Dimopoulos, A. Hook, J. Huang, and G. Marques-Tavares, A collider observable QCD axion, J. High Energy Phys. 11 (2016) 052.

[32] P. Agrawal and K. Howe, Factoring the strong *CP* problem, J. High Energy Phys. 12 (2018) 029.

[33] P. Agrawal, G. Marques-Tavares, and W. Xue, Opening up the QCD axion window, J. High Energy Phys. 03 (2018) 049.

[34] M. K. Gaillard, M. B. Gavela, R. Houtz, P. Quilez, and R. Del Rey, Color unified dynamical axion, Eur. Phys. J. C **78**, 972 (2018).

[35] A. Hook, S. Kumar, Z. Liu, and R. Sundrum, High Quality QCD Axion and the LHC, Phys. Rev. Lett. **124**, 221801 (2020).

[36] T. Gherghetta, V. V. Khoze, A. Pomarol, and Y. Shirman, The axion mass from 5D small instantons, J. High Energy Phys. 03 (2020) 063.

[37] R. S. Gupta, V. V. Khoze, and M. Spannowsky, Small instantons and the strong *CP* problem in composite Higgs models, arXiv:2012.00017.

[38] A. Mariotti, D. Redigolo, F. Sala, and K. Tobioka, New LHC bound on low-mass diphoton resonances, Phys. Lett. B **783**, 13 (2018).

[39] M. Kamionkowski and J. March-Russell, Planck scale physics and the Peccei-Quinn mechanism, Phys. Lett. B **282**, 137 (1992).

[40] R. Holman, S. D. H. Hsu, T. W. Kephart, E. W. Kolb, R. Watkins, and L. M. Widrow, Solutions to the strong *CP* problem in a world with gravity, Phys. Lett. B **282**, 132 (1992).

[41] S. M. Barr and D. Seckel, Planck scale corrections to axion models, Phys. Rev. D **46**, 539 (1992).

[42] S. Ghigna, M. Lusignoli, and M. Roncadelli, Instability of the invisible axion, Phys. Lett. B **283**, 278 (1992).

[43] D. Aloni, Y. Soreq, and M. Williams, Coupling QCD-Scale Axionlike Particles to Gluons, Phys. Rev. Lett. **123**, 031803 (2019).

[44] H. Georgi, D. B. Kaplan, and L. Randall, Manifesting the invisible axion at low-energies, Phys. Lett. **169B**, 73 (1986).

[45] W. A. Bardeen, R. D. Peccei, and T. Yanagida, Constraints on variant axion models, Nucl. Phys. **B279**, 401 (1987).

[46] D. S. M. Alves and N. Weiner, A viable QCD axion in the MeV mass range, J. High Energy Phys. 07 (2018) 092.

[47] S. Gori, G. Perez, and K. Tobioka, KOTO vs NA62 dark scalar searches, J. High Energy Phys. 08 (2020) 110.

[48] A. V. Artamonov *et al.* (E949 Collaboration), Search for the decay K+ to pi + gamma gamma in the pi + momentum region P > 213 MeV/c, Phys. Lett. B **623**, 192 (2005).

[49] C. Lazzeroni *et al.* (NA62 Collaboration), Study of the $K^{\pm} \to \pi^{\pm}\gamma\gamma$ decay by the NA62 experiment, Phys. Lett. B **732**, 65 (2014).

[50] E. Abouzaid *et al.* (KTeV Collaboration), Final results from the KTeV experiment on the decay $K_L \to \pi^0\gamma\gamma$, Phys. Rev. D **77**, 112004 (2008).

[51] J. K. Ahn *et al.* (KOTO Collaboration), Search for the $K_L \to \pi^0\nu\bar{\nu}$ and $K_L \to \pi^0 X^0$ Decays at the J-PARC KOTO Experiment, Phys. Rev. Lett. **122**, 021802 (2019).

[52] M. Bauer, M. Neubert, S. Renner, M. Schnubel, and A. Thamm, Consistent treatment of axions in the weak chiral Lagrangian, arXiv:2102.13112.

[53] A. Aguilar-Arevalo *et al.* (PIENU Collaboration), Search for heavy neutrinos in $\pi \to \mu\nu$ decay, Phys. Lett. B **798**, 134980 (2019).

[54] D. Pocanic *et al.*, Precise Measurement of the pi+ → pi0 e + nu Branching Ratio, Phys. Rev. Lett. **93**, 181803 (2004).

[55] W. Altmannshofer, S. Gori, and D. J. Robinson, Constraining axionlike particles from rare pion decays, Phys. Rev. D **101**, 075002 (2020).

[56] H. Al Ghoul *et al.* (GlueX Collaboration), Measurement of the beam asymmetry Σ for π^0 and η photoproduction on the proton at $E_\gamma = 9$ GeV, Phys. Rev. C **95**, 042201 (2017).

[57] D. Aloni, C. Fanelli, Y. Soreq, and M. Williams, Photoproduction of Axionlike Particles, Phys. Rev. Lett. **123**, 071801 (2019).

[58] G. Abbiendi *et al.* (OPAL Collaboration), Multiphoton production in e+e− collisions at s∗∗(1/2) = 181 − GeV to 209-GeV, Eur. Phys. J. C **26**, 331 (2003).

[59] S. Knapen, T. Lin, H. K. Lou, and T. Melia, Searching for Axionlike Particles with Ultraperipheral Heavy-Ion Collisions, Phys. Rev. Lett. **118**, 171801 (2017).

[60] A. M. Sirunyan *et al.* (CMS Collaboration), Search for low mass vector resonances decaying into quark-antiquark pairs in proton-proton collisions at $\sqrt{s} = 13$ TeV, J. High Energy Phys. 01 (2018) 097.

[61] M. Tanabashi *et al.* (Particle Data Group Collaboration), Review of particle physics, Phys. Rev. D **98**, 030001 (2018).

[62] X. Cid Vidal, A. Mariotti, D. Redigolo, F. Sala, and K. Tobioka, New axion searches at flavor factories, J. High Energy Phys. 01 (2019) 113.

[63] X. Cid Vidal *et al.*, Report from Working Group 3: Beyond the Standard Model physics at the HL-LHC and HE-LHC, CERN Yellow Rep. Monogr. **7**, 585 (2019).

[64] E. Izaguirre, T. Lin, and B. Shuve, Searching for Axionlike Particles in Flavor-Changing Neutral Current Processes, Phys. Rev. Lett. **118**, 111802 (2017).

[65] M. B. Gavela, R. Houtz, P. Quilez, R. Del Rey, and O. Sumensari, Flavor constraints on electroweak ALP couplings, Eur. Phys. J. C **79**, 369 (2019).

[66] M. Bauer, M. Neubert, S. Renner, M. Schnubel, and A. Thamm, The low-energy effective theory of axions and ALPs, J. High Energy Phys. 04 (2021) 063.

[67] M. Bauer, M. Neubert, and A. Thamm, Collider probes of axion-like particles, J. High Energy Phys. 12 (2017) 044.

[68] M. Chala, G. Guedes, M. Ramos, and J. Santiago, Running in the ALPs, Eur. Phys. J. C **81**, 181 (2021).

[69] B. Batell, M. Pospelov, and A. Ritz, Multi-lepton signatures of a hidden sector in rare B decays, Phys. Rev. D **83**, 054005 (2011).

[70] P. Ball and R. Zwicky, New results on $B \to \pi, K, \eta$ decay form factors from light-cone sum rules, Phys. Rev. D **71**, 014015 (2005).

[71] P. Ball and R. Zwicky, $B_{d,s} \to \rho, \omega, K^*, \phi$ decay form-factors from light-cone sum rules revisited, Phys. Rev. D **71**, 014029 (2005).

[72] P. Zyla *et al.* (Particle Data Group Collaboration), Review of particle physics, Prog. Theor. Exp. Phys. **2020**, 083C01 (2020).

[73] V. Chobanova *et al.* (Belle Collaboration), Measurement of branching fractions and *CP* violation parameters in $B \to \omega K$ decays with first evidence of *CP* violation in $B^0 \to \omega K_S^0$, Phys. Rev. D **90**, 012002 (2014).

[74] J. Lees *et al.* (*BABAR* Collaboration), Measurements of branching fractions and *CP* asymmetries and studies of angular distributions for B → phi phi K decays, Phys. Rev. D **84**, 012001 (2011).

[75] B. Aubert *et al.* (*BABAR* Collaboration), Study of B Meson Decays with Excited eta and eta-prime Mesons, Phys. Rev. Lett. **101**, 091801 (2008).

[76] R. Aaij *et al.* (LHCb Collaboration), Study of B_c^+ decays to the $K^+K^-\pi^+$ final state and evidence for the decay $B_c^+ \to \chi_{c0}\pi^+$, Phys. Rev. D **94**, 091102 (2016).

[77] Y. Gershtein, S. Knapen, and D. Redigolo, Probing naturally light singlets with a displaced vertex trigger, arXiv:2012.07864.

[78] K. J. Kelly, S. Kumar, and Z. Liu, Heavy axion opportunities at the DUNE near detector, Phys. Rev. D **103**, 095002 (2021).

[79] J. Beacham *et al.*, Physics beyond colliders at CERN: Beyond the standard model working group report, J. Phys. G **47**, 010501 (2020).

[80] J. Vermaseren, New features of FORM, arXiv:math-ph/0010025.

[81] P. Maierhofer, J. Usovitsch, and P. Uwer, Kira—A Feynman integral reduction program, Comput. Phys. Commun. **230**, 99 (2018).

[82] C. Balzereit, T. Mannel, and B. Plumper, The renormalization group evolution of the CKM matrix, Eur. Phys. J. C **9**, 197 (1999).

[83] P. Marquard, A. V. Smirnov, V. A. Smirnov, and M. Steinhauser, Quark Mass Relations to Four-Loop Order in Perturbative QCD, Phys. Rev. Lett. **114**, 142002 (2015).